J|A|C|S
ARTICLES
Published on Web 01/27/2004

Selective Metallic Tube Reactivity in the Solution-Phase Osmylation of Single-Walled Carbon Nanotubes

Sarbajit Banerjee[†] and Stanislaus S. Wong*[,†,‡]

Contribution from the Department of Chemistry; State University of New York at Stony Brook; Stony Brook, New York 11794-3400, and Materials and Chemical Sciences Department, Brookhaven National Laboratory; Building 480; Upton, New York 11973

Received August 25, 2003; E-mail: sswong@notes.cc.sunysb.edu; sswong@bnl.gov

Abstract: Single-walled carbon nanotubes have been reacted with osmium tetroxide (OsO_4) in solution in the presence of O_2 and UV irradiation at 254 nm. We observe one main structural motif, namely thickly coated nanotube structures, densely covered with OsO_2, consisting of multiple bundles of derivatized tubes. In a few instances, bridging uncoated tubes, connecting these thickly coated structures, incorporate a number of smaller nanotube bundles, projecting out from the larger functionalized aggregates of tubes. It is believed that OsO_2 (a) initially forms on the nanotubes by the preferential covalent sidewall functionalization of metallic nanotubes and (b) subsequently self-aggregates. The formation of an intermediate charge-transfer complex is likely the basis for the observed selectivity and reactivity of metallic tubes. Extensive characterization of these osmylated adducts has been performed using a variety of electron microscopy and optical spectroscopy techniques.

Introduction

In recent years, single-walled carbon nanotubes (SWNTs) have emerged as significant building blocks in nanoscale technology. Their unique structure-dependent mechanical and electronic properties[1] make them of interest in fundamental science. For instance, the combination of the helicity and diameter of SWNTs, defined by the roll-up vector, often determines whether a tube is a metal or a semiconductor.[1] They are thought to have a host of wide-ranging, potential applications including as catalyst supports in heterogeneous catalysis, field emitters, high strength engineering fibers, sensors, actuators, tips for scanning probe microscopy, gas storage media, and molecular wires for the next generation of electronic devices.[2−8]

The generation of such nanotube-based structures requires the development of rational nanotube chemistry. Chemical modification is also essential to deposition of catalysts and other species onto nanotube surfaces for nanocatalytic and sensor applications. Functionalization of carbon nanotubes and the generation of nanotube-based composites have recently drawn a lot of attention.[9−12] Nanotube sidewalls, end caps, defect sites, and interiors have been extensively targeted for chemical derivatization to generate new families of materials with interesting properties.[9,12,13] We and others have noted that much of nanotube chemistry has been different and even more challenging than that of close structural analogues, such as fullerenes (C_{60}).[12]

Our previous work has focused on the role of carbon nanotubes as chemical ligands with distinctive sites for molecular modification,[11,14−17] and we have demonstrated the use of these functionalized nanotubes for applications, such as catalyst support media.[16,18] What we propose in this study is the use of a chemical reaction, i.e., solution-phase osmylation, to enable the differentiation and separation of metallic and semiconducting tubes from as-prepared tubes. Separation of SWNTs, according to their electronic characteristics, is essential to the development of molecular electronics, including field-effect transistors. Recent efforts by other groups have used noncovalent and covalent sidewall chemistry to probe differential reactivity in metallic and semiconducting nanotubes.[19−22] These chemically based

[†] State University of New York at Stony Brook.
[‡] Brookhaven National Laboratory.

(1) Dresselhaus, M. S.; Dresselhaus, G.; Avouris, P. *Carbon Nanotubes: Synthesis, Structure, Properties, and Applications*; Springer-Verlag: Berlin, 2001.
(2) Bachtold, A.; Hadley, P.; Nakanshi, T.; Dekker, C. *Science* **2001**, *294*, 1317.
(3) Planeix, J. M.; Coustel, N.; Coq, B.; Brotons, V.; Kumbhar, P. S.; Dutartre, R.; Geneste, P.; Bernier, P.; Ajayan, P. M. *J. Am. Chem. Soc.* **1994**, *116*, 7935.
(4) Baughman, R. H.; Cui, C.; Zakhidov, A. A.; Iqbal, Z.; Barisci, J. N.; Spinks, G. M.; Wallace, G. G.; Mazzoldi, A.; De Rossi, D.; Rinzler, A. G.; Jachinski, O.; Roth, S.; Kertesz, M. *Science* **1999**, *284*, 1340.
(5) Fan, S.; Chapline, M. G.; Franklin, N. R.; Tombler, T. W.; Cassell, A. M.; Dai, H. *Science* **1999**, *283*, 512.
(6) Kong, J.; Franklin, N. R.; Zhou, C.; Chapline, M. G.; Peng, S.; Cho, K.; Dai, H. *Science* **2000**, *287*, 622.
(7) Wong, S. S.; Woolley, A. T.; Joselevich, E.; Cheung, C. L.; Lieber, C. M. *J. Am. Chem. Soc.* **1998**, *120*, 8557.
(8) Avouris, P. *Acc. Chem. Res.* **2002**, *35*, 1026.
(9) Hirsch, A. *Angew. Chem., Intl. Ed.* **2002**, *41*, 1853.
(10) Bahr, J.; Tour, J. M. *J. Mater. Chem.* **2002**, *12*, 1952.
(11) Banerjee, S.; Kahn, M. G. C.; Wong, S. S. *Chem. Eur. J.* **2003**, *9*, 1898.
(12) Niyogi, S.; Hamon, M. A.; Hu, H.; Zhao, B.; Bhowmik, P.; Sen, R.; Itkis, M. E.; Haddon, R. C. *Acc. Chem. Res.* **2002**, *35*, 1105.
(13) Sinnott, S. B. *J. Nanosci. Nanotech.* **2002**, *2*, 113.
(14) Banerjee, S.; Wong, S. S. *J. Phys. Chem. B* **2002**, *106*, 12144.
(15) Banerjee, S.; Wong, S. S. *Nano Lett.* **2002**, *2*, 195.
(16) Banerjee, S.; Wong, S. S. *J. Am. Chem. Soc.* **2002**, *124*, 8940.
(17) Kahn, M. G. C.; Banerjee, S.; Wong, S. S. *Nano Lett.* **2002**, *2*, 1215.
(18) Banerjee, S.; Wong, S. S. *Nano Lett.* **2002**, *2*, 49.
(19) Chen, Z.; Du, X.; Du, M.-H.; Rancken, C. D.; Cheng, H.-P.; Rinzler, A. G. *Nano Lett.* **2003**, *3*, 1245.
(20) Chattopadhyay, D.; Galeska, I.; Papadimitrakopoulos, F. *J. Am. Chem. Soc.* **2003**, *125*, 3370.
(21) Strano, M. S. *J. Am. Chem. Soc.* **2003**, *125*, 16148.

methods seem more promising to effect the bulk separation of tubes, as compared with techniques associated with (i) alternating current dielectrophoresis and (ii) the current-induced oxidation of metallic nanotubes, which have recently been reported as alternative methods of achieving chiral separations of nanotubes.[23,24] Exploration of these types of reactions (e.g., osmylation) is critical for the development of interesting chemical and physical properties at the interface between molecules and materials as well as for establishing protocols for the selective functionalization of nanotubes. In fact, these experiments may have bearing on creating methods for obtaining size and chiral selectivity of SWNTs.

Significance of Nanotube "Osmylation". The present study focuses on a comprehensive, interdisciplinary approach to understanding osmylation of carbon nanotubes. That is, we are interested in the precise structural interactions involved in the controlled reaction between single-walled carbon nanotubes (SWNTs) and osmium tetroxide (OsO_4). OsO_4 is widely used to convert olefins into diols.[25] Specifically, of high importance to organic synthesis, OsO_4 has been employed to catalyze asymmetric aminohydroxylation as well as asymmetric dihydroxylation.[26] Osmylation of fullerenes is well understood. In the presence of pyridine, a well-characterized product, consisting of an osmate ester that retained the intrinsic fullerene framework, could be isolated.[27] In fact, osmylation has been used to grow single crystals of C_{60} for structure elucidation and to achieve kinetic resolution of chiral fullerenes.[27−30]

However, osmylation of carbon nanotubes has been far more complex. Theoretical predictions based on the ONIOM model indicate that osmate esters form via a covalent linkage of OsO_4 with the double bonds on the tube sidewalls through a reaction catalyzed by the presence of base.[31a] Another report suggested that the ends of multiwalled nanotubes were opened when they were treated with OsO_4.[32] A recent experiment illustrated a dramatic increase in the electrical resistance of metallic carbon nanotubes in the presence of OsO_4 vapors and an O_2 atmosphere with UV irradiation.[31b] The authors interpreted this phenomenon as arising from covalent functionalization and cycloaddition of OsO_4 to the carbon lattice with formation of the postulated osmate ester.[31b] We believe, though, that in and of themselves conductivity measurements alone are insufficient evidence for the presence of a covalent linkage. More extensive structural characterization is necessary to fully establish the precise chemical nature of the metal−nanotube interaction.[10]

To understand and define this interaction more clearly, we have studied an analogous, though nonreversible, reaction using solution-phase OsO_4 in the presence of UV irradiation. In effect, our results strongly indicate that the interaction of SWNTs with OsO_4 leads to the reduction of the Os(VIII) species and the formation of nanocrystalline OsO_2 on the surfaces of tubes. The OsO_2 nanoparticles may be said to have "templated" onto the nanotubes, likely by selective covalent sidewall functionalization of metallic tubes in particular. Moreover, they probably are also deposited inside the bundles of tubes and in the interstitial channels between the tubes. From microscopy data, it is evident that they thoroughly cover and are dispersed along the nanotube sidewalls. Moreover, the OsO_2 clusters aggregate the nanotubes into thick bundles. Herein, we present extensive structural characterization for adducts of SWNT−OsO_4 interaction and propose viable mechanisms and bonding modes. This particular reaction methodology yields different particle stacking behavior and particle densities on SWNTs from previous covalent functionalization attempts, aimed at tethering of nanocrystalline particles to the ends and defect sites of tubes.[15,33−36] Osmylation is clearly a unique reaction process of SWNTs and delineates some of the challenges associated with site-specific tube functionalization.

Experimental Section

Synthesis of Osmylated Adducts. Raw SWNTs (HiPco, Carbon Nanotechnologies Inc.) were purified by mild oxidation in wet air followed by treatment with HCl, copious washing with water, and drying at high temperature.[37] This treatment is able to remove a significant portion (though not all) of the remnant HiPco iron catalyst.

In the functionalization reaction, 13.5 mg of the purified SWNTs was mixed with a large excess of OsO_4 (Aldrich, 184 mg) and dispersed in 10 mL of toluene by brief sonication. Aliquots from this mixture were placed in a quartz cell with a 10 mm path length and irradiated with 254 nm light from a 200 W Hg arc lamp (Oriel instruments). A band-pass filter was used at 254 nm to block out all other wavelengths. Mixtures were irradiated for approximately 2 h with extensive stirring. Workup for the reaction involved filtration over a 0.2 μm PTFE membrane, followed by washing with ample quantities of toluene and methanol. Control experiments involved the systematic elimination of nanotubes, OsO_4, or UV irradiation, respectively, from the reaction mixture.

Scanning Electron Microscopy. Samples for SEM were drop dried onto 300 mesh Cu grids covered with lacy carbon film. The grids were placed on a homemade sample holder and held over a Be plate. They were imaged using a Leo 1550 field emission instrument at accelerating voltages from 2 to 10 kV at a working distance of 2 mm. It is of note that all samples, including the functionalized adducts, could be imaged as is, without the need for additional metal sputter coating.

Transmission Electron Microscopy. Samples were drop dried on the grids from solution. Low-resolution images were obtained on a Philips CM12 TEM, equipped with enrgy-dispersive X-ray spectroscopic (EDS) capabilities at accelerating voltages of 120 kV. High-resolution images were obtained on a JEOL 2010F instrument equipped with an INCA EDS system, at accelerating voltages of 200 kV.

X-ray Photoelectron Spectroscopy. For XPS analyses, the samples were attached to stainless steel holders using conductive double-sided tape, and placed in the vacuum chamber of a Model DS800 XPS surface analysis system (Kratos Analytical Plc, Manchester, UK). The chamber was evacuated to a base pressure of $\sim 5 \times 10^{-9}$ Torr. A hemispherical energy analyzer was used for electron detection. XPS spectra were first

(22) Strano, M. S.; Dyke, C. A.; Usrey, M. L.; Barone, P. W.; Allen, M. J.; Shan, H.; Kittrell, C.; Hauge, R. H.; Tour, J. M.; Smalley, R. E. *Science* **2003**, *301*, 1519.
(23) Collins, P. G.; Arnold, M. S.; Avouris, P. *Science* **2001**, *292*, 706.
(24) Krupke, R.; Hennrich, F.; Lohneysen, H. V.; Kappes, M. M. *Science* **2003**, *301*, 344.
(25) Schroeder, M. *Chem. Rev.* **1980**, *80*, 187.
(26) Sharpless, K. B. *Angew. Chem., Int. Ed.* **2002**, *41*, 2024.
(27) Hawkins, J. M.; Lewis, T. A.; Loren, S. D.; Meyer, A.; Heath, J. R.; Shibato, Y.; Saykally, R. J. *J. Org. Chem.* **1990**, *55*, 6250.
(28) Hawkins, J. M. *Acc. Chem. Res.* **1992**, *25*, 150.
(29) Hawkins, J. M.; Meyer, A.; Lewis, T. A.; Loren, S.; Hollander, F. J. *Science* **1991**, *252*, 312.
(30) Hawkins, J. M.; Meyer, A. *Science* **1993**, *260*, 1918.
(31) (a) Lu, X.; Tian, F.; Feng, Y.; Xu, X.; Wang, N.; Zhang, Q. *Nano Lett.* **2002**, *2*, 1325. (b) Cui, J.; Burghard, M.; Kern, K. *Nano Lett.* **2003**, *3*, 615.
(32) Hwang, K. C. *Chem. Commun.* **1995**, 173.
(33) Banerjee, S.; Wong, S. S. *J. Am. Chem. Soc.* **2003**, *125*, 10342.
(34) Ravindran, S.; Chaudhary, S.; Colburn, B.; Ozkan, M.; Ozkan, C. S. *Nano Lett.* **2003**, *3*, 447.
(35) Azamaian, B. R.; Coleman, K. S.; Davis, J.; Hanson, N.; Green, M. L. H. *Chem. Commun.* **2002**, 366.
(36) Haremza, J. M.; Hahn, M. A.; Krauss, T. D.; Chen, S.; Calcines, J. *Nano Lett.* **2002**, *2*, 1253.
(37) Bahr, J. L.; Tour, J. M. *Chem. Mater.* **2001**, *13*, 3823.

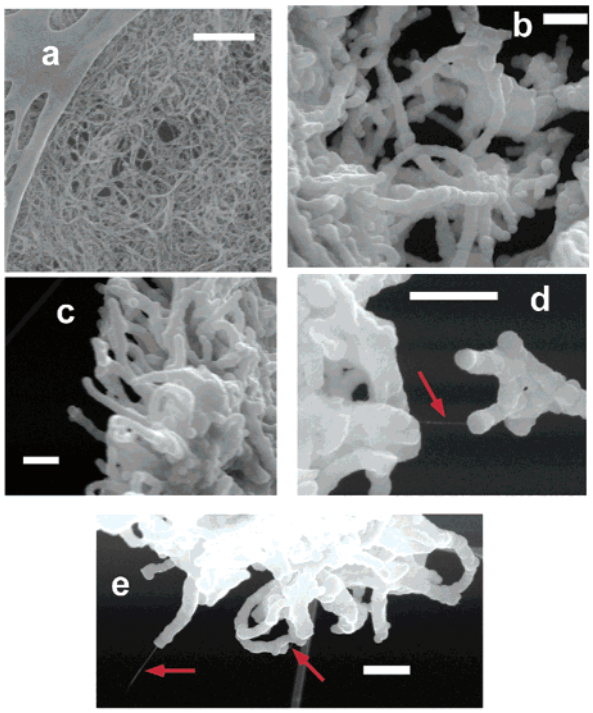

Figure 1. Scanning electron micrographs. (a) Purified HiPco SWNTs. (b and c) Aggregates of osmium dioxide templated SWNT bundles. (d) Metal oxide coated SWNT bundles. These are seen in high resolution in Figure 4. (e) Partially uncoated nanotube bundles protruding from OsO_2-coated templated aggregates. Red arrows in (d) and (e) depict nanotube bundles, where the metal coating is not completely covering all of the nanotubes. Scale bar represents 400 nm in each case.

collected using a Mg Kα X-ray source at 80 eV pass energy and in 0.75 eV steps. High-resolution spectra were collected at pass energy of 10 eV and in 0.1 eV steps.

Raman Spectroscopy. FT-Raman spectra were obtained on a Brüker instrument on dispersions of nanotubes in DMF or CS_2. The Raman data were acquired, after 100−200 scans, upon excitation of a 1064 nm Nd:YAG laser at a power of ∼100 mW, using a liquid N_2 cooled Ge detector. For Raman microprobe measurements, samples were drop cast onto Si wafers. Spectra were collected at 632.8 nm excitation (He−Ne laser at ∼5 mW) and at 514.5 nm (Ar ion laser at 2−3 mW) on a Kaiser Raman and a Reinshaw System 1000 microscope, respectively. The spectra were acquired at resolutions superior to 2 cm^{-1}.

Optical Spectroscopy. Samples were dispersed in *o*-dichlorobenzene (ODCB) or in DMF by mild and brief sonication. Clear solutions were obtained by filtering over glass wool. UV−visible spectra were obtained on a Thermospectronics UV1 instrument using quartz cells with a 10 mm path length at a resolution of 1 nm. FT-near-IR data were obtained on a Nexus 670 (Thermo Nicolet) instrument equipped with a single-reflectance ZnSe ATR accessory, a CaF_2 beam splitter, and a InGaAs detector. Samples were placed on a ZnSe crystal. Data were taken at a reproducible pressure.

Results and Discussion

Microscopy Characterization. Figure 1a shows purified HiPco tubes. Figure 1b−e shows SEMs of nanotubes that have been reacted with OsO_4. The gross tubular morphology is preserved. However, the tubes are thickly coated with clumps of OsO_2. EDS measurements in the SEM showed a strong osmium signal consistent with the expected formation of this coating. These images show that the metal coating is neither sharply faceted nor single crystalline. Sections of single nanotubes or bundles can sometimes be observed where the coating has not completely enveloped the tubes. As mentioned earlier, these images indicate a different reaction mechanism from previous reports of nanotube−nanocrystal adduct formation,[15,33−36] where isolated, discrete particles have attached at defect sites and ends. In this case, there is essentially complete coverage of nanoparticles on the nanotube sidewalls, suggesting their mediation in this reaction.

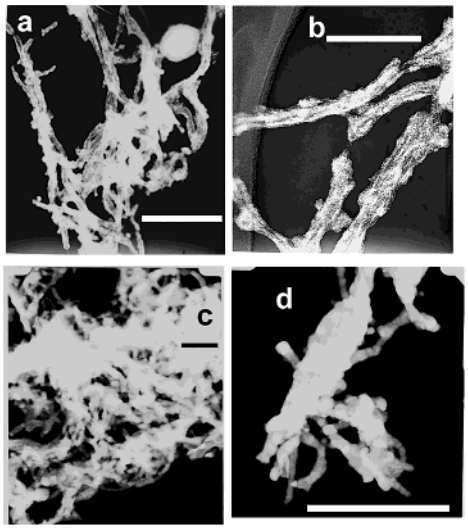

Figure 2. (a) Low-resolution TEM image of partially coated tubes, functionalized with OsO_2. The UV irradiation time used was ∼90 min. Scale bar represents 300 nm. (b) Higher magnification TEM image of tubes in (a), showing particulate nature of the tube coating. Scale bar is 125 nm. (c) Low-resolution TEM image of aggregate of more thickly OsO_2 coated tubes. The irradiation time is ∼2 h. Scale bar is 500 nm. (d) Higher magnification image of bundles of thickly coated tubes after ∼2 h irradiation time. Scale bar is 500 nm. Note the high electron contrast due to Os.

In Figure 2a,b are low-resolution TEM images of osmylated tubes that have been UV irradiated for about 90 min. Small grains strung along the nanotube bundles can be observed covering a large proportion of the nanotube sidewalls. In Figure 2c,d, with UV irradiation for ∼2 h, the coverage is denser and the coating of small individual OsO_2 particles is effectively continuous along the sidewalls. Due to the confirmed elemental presence of osmium, all of the electron microscopy images discussed above show significantly higher contrast for the functionalized species as compared with the nanotubes themselves.

Figure 3a−e contains high-resolution TEM (HRTEM) images of the modified nanotubes. The particles are intercalated between the bundles and deposited along the sides of the bundles. Most of the particles are not larger than 2 nm, and some show tiny crystalline cores, while other particles appear amorphous. EDS spectra, shown in Figure 3f, show the expected Os and O signals for these particles. As is evident in Figure 3a,b,d, the particles are deposited inside bundles as well as coat the outer surfaces of the bundles. Figure 3c shows deposition of tiny particles with resolvable lattice fringes onto a small bundle of tubes. These OsO_2 particles seem to be able to adjoin several tubes and even several bundles of tubes together to form the structures seen in Figure 1b−d. It is of note that the oxide is present in an X-ray amorphous form. The few diminutive crystalline cores of these particles, observed in HRTEM, are too small to produce a distinctive X-ray diffraction pattern.

Figure 4 shows high-resolution TEM images of isolated, uncoated tubes, which had initially been delineated by the red

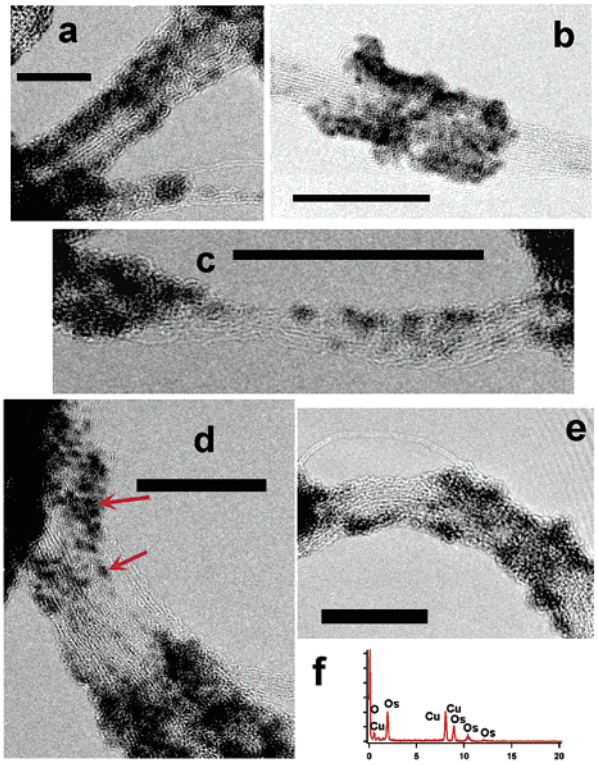

Figure 3. High-resolution TEM images of partially coated, metal oxide functionalized tubes. (a) Most of the OsO_2 particles are amorphous and are deposited on the sidewalls. (b) Clumped deposition of OsO_2 on top of bundles as well as between the tubes of the bundles. (c) Particles with tiny crystalline cores are visible on the tubes. (d) A mixture of crystalline and amorphous particles, deposited on the surfaces of bundles and between tubes. Red arrows refer to typical crystalline particles. (e) Some functionalized tubes appear to be partially exfoliated from the larger aggregate bundle. Scale bars are 20 nm in each case, except for (a) where the scale bar represents 10 nm. (f) EDS spectrum of a typical functionalized nanotube aggregate. Horizontal axis is energy in keV.

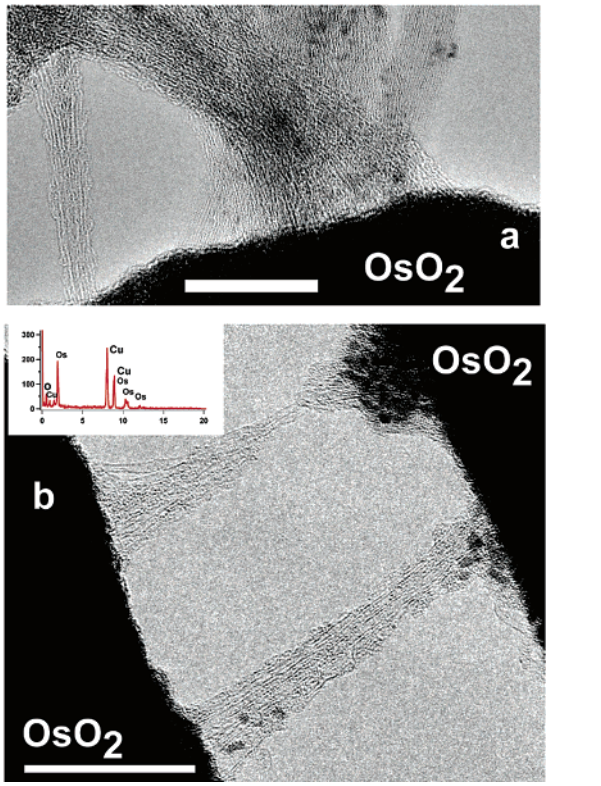

Figure 4. High-resolution TEM images of isolated, uncoated tubes, which had initially been delineated by the red arrows in Figure 1, protruding from the thick, aggregated clumps of osmium oxide coating the nanotube structures. (a) Tubes projecting from a bulky OsO_2-coated nanotube bundle. Several bundles of tubes appear to be held together in these thickly aggregated structures. (b) SWNT bundles connecting and protruding from two broad OsO_2-coated nanotube aggregates. Inset: EDS spectrum showing the presence of Os. Horizontal axis is energy in keV. Scale bars are 20 nm in each case.

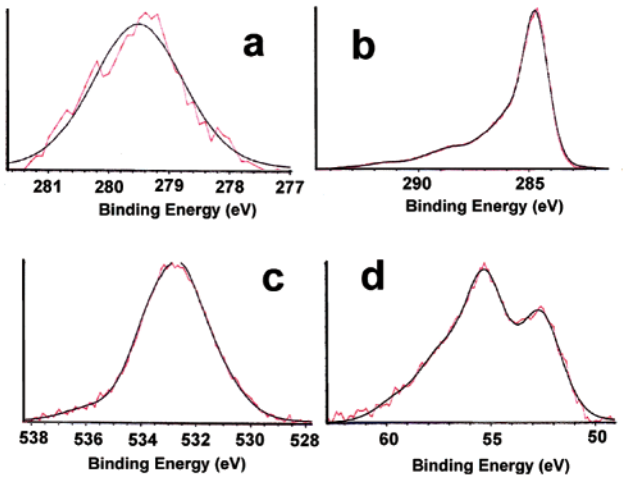

Figure 5. High-resolution XPS spectra of functionalized nanotube aggregates (red) as well as the fit (black). Bottom axis represents binding energy (in eV). (a) Os 4d region; (b) C 1s region; (c) O 1s region; (d) Os 4f region.

arrows in Figure 1, protruding from the thick, aggregated clumps of osmium oxide coating the nanotube structures. It is evident from these images that (a) the thickly coated structures, labeled OsO_2 in Figure 4, consist of multiple bundles of derivatized tubes and that (b) the bridging uncoated tubes, connecting these thickly coated structures, incorporate a number of smaller nanotube bundles, projecting from the larger functionalized aggregates of tubes.

Such coated ropes are similar to previously described SiO_2 or SnO coated nanotube structures reported in the literature.[38,39] However, there is a major difference. In those previous experiments, the oxide particles were preformed by various wet solution routes and allowed to deposit onto the surfaces of nanotubes; the nanotubes did not chemically mediate the nanoparticle formation. In contrast, in our experiment, as will be discussed in more detail in later sections, the nanotube itself plays an important chemical role in determining the nature and distribution of osmium oxide particles, which form spontaneously upon UV irradiation.

XPS Characterization. High-resolution XPS spectra (Figure 5) of the functionalized tubes identified Os to consist almost exclusively of the nanoparticulate OsO_2 form, where the Os metal retains an oxidation state of +4. Since OsO_2 itself is conducting,[40] no charging neutralization was required for any of the measurements described. The Os $4d_{5/2}$ peak could be fit with a single line centered at a binding energy of 279.49 eV (Figure 5a). This peak is distinct from the C 1s peak at 284.5

(38) Han, W.-Q.; Zettl, A. *Nano Lett.* **2003**, *3*, 681.
(39) Whitsitt, E. A.; Barron, A. R. *Nano. Lett.* **2003**, *3*, 775.
(40) Hayakawa, Y.; Fukuzaki, K.; Kohiki, S.; Shibata, Y.; Matsuo, T.; Wagatsuma, K.; Oku, M. *Thin Solid Films* **1999**, *347*, 56.

eV (Figure 5b). In fact, in the C 1s spectrum, shown in Figure 5b, the high-energy tail can be fitted to an osmium $4d_{3/2}$ peak at 293.12 eV. Moreover, the C 1s spectrum also shows contributions from oxygenated functionalities, including those introduced during the purification step, as well as those produced by oxidation of the nanotube by OsO_4. The Os $4f_{7/2}$ and $4f_{5/2}$ peaks (Figure 5d) contain a limited contribution from the Fe $3p_{1/2}$ and $3p_{3/2}$ peaks, originating from remnant HiPco catalyst. From peak shape analysis, an OsO_2 component, composed of contributions at 52.57 and 55.29 eV, could be identified. The assigned values are consistent with those observed in the literature.[40] The O 1s spectrum (Figure 5c) showed contributions from the metal oxide (531 eV) as well as from the oxygenated functional groups on the nanotube.

Raman Discussion: Evidence for Selective Reactivity of Metallic Tubes. Raman spectroscopy is a particularly sensitive probe of electronic and vibrational structure and their coupling in SWNTs.[41] Raman spectra for different sets of carbon nanotubes are resonantly enhanced at selected laser excitation wavelengths due to coupling with the optically allowed electronic transitions between the van Hove singularities in the electronic density of states of the SWNTs. Characteristic features of the Raman spectrum of SWNTs include the diameter-dependent radial breathing modes (RBM)[42] (150−300 cm^{-1}), the tangential mode or G band (~1560−1600 cm^{-1}), and the disorder-induced D band (~1290−1320 cm^{-1}). Importantly for this work, the shape and intensity of a disorder mode peak have been correlated with the extent of nanotube sidewall functionalization.[22,37]

Sidewall functionalization is accompanied by the formation of sp^3-hybridized carbons on the sidewalls and therefore substantial disruption of electronic structure. This leads to a significant increase in the disorder band and is often used as a probe for site specificity and selectivity of a functionalization reaction.[10,14,37] In general, though, with increasing extent of sidewall functionalization, as the pseudo one-dimensional lattice becomes increasingly disrupted, the nanotubes are no longer in electronic resonance, and thus, the intensities of all the peaks sharply decrease.[22]

FT-Raman spectra for nanotubes are shown in Figure 6. The excitation energy dependence of the I_G/I_D ratio has previously been fitted[43] to eq 1:

$$I_G/I_D = 10.6 + 0.06e^{E/0.46} \quad (1)$$

where E is the laser excitation energy in eV.

Thus, at 1064 nm (1.165 eV) laser excitation, this ratio is expected to be low; hence, an increase in the D band intensity upon sidewall functionalization should be clearly apparent. Figure 6a shows the D and G band regions. At 1064 nm, primarily semiconducting tubes are excited[44] and the G band consists of the longitudinal and transversal components of the lattice C−C stretching vibrations of E_2, A, and E_1 symmetries. It is evident that there is no substantial increase in the relative intensity of the D band upon reaction with OsO_4 and that the structural integrity of the sidewalls associated with semiconducting tubes is mainly preserved.

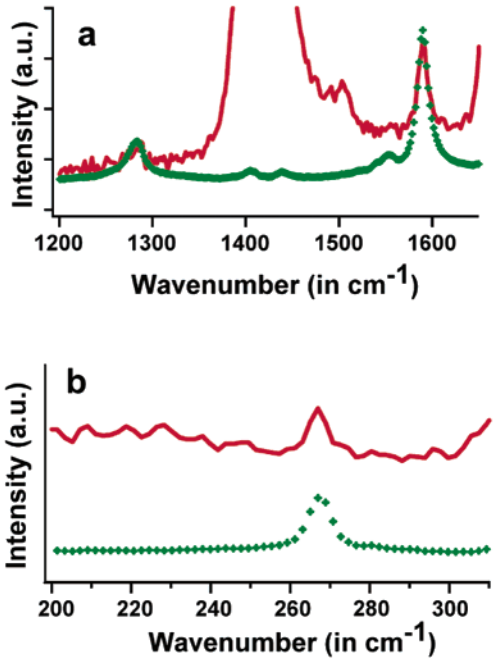

Figure 6. FT-Raman spectra of functionalized nanotube aggregates. (a) G and D band regions of purified tubes (green markers) and OsO_2-derivatized tubes (red). The large peak in the central region of the spectrum of the functionalized tubes is associated with the DMF solvent. This feature is not as apparent in the spectrum of purified tubes, which may be due to concentration effects. (b) Radial breathing mode region in the FT spectra of purified tubes (green markers) and OsO_2-derivatized tubes (red).

The RBM region shown in Figure 6b provides further evidence for the presence of SWNTs and their structural integrity in the composite. A single peak at 267 cm^{-1} is noted in the FT-Raman spectra. The RBM frequency is related to the diameter as follows:

$$\omega_{RBM}/cm^{-1} = C_1/d + C_2 \quad (2)$$

Using 239 and 8.5 wavenumbers as values of C_1 and C_2, based on literature reports of multilaser studies of HiPco tubes,[43] these calculations would yield relatively small diameter semiconducting tubes with a diameter of ~0.92 nm.

Figure 7 shows the Raman microprobe measurements obtained using He−Ne laser excitation at 632.8 nm (1.96 eV). Compared to the spectra of the purified tubes, the small downshift in the G band position and the attenuation of the D band intensity (Figure 7a), upon UV irradiation, noted in the spectra of osmylated tubes, can be attributed to the removal of p-doping, as oxygen is desorbed from the nanotubes.[45] At this excitation wavelength, larger diameter metallic and smaller diameter semiconducting tubes are primarily observed.[21] In addition, a G band shoulder corresponding to Breit−Wagner−Fano (BWF) broadened lines, associated with metallic tubes, has started to appear as a low-energy tail. The BWF asymmetric shape is due to the coupling of phonons and electrons in metallic tubes.[42] Figure 7b shows the RBM region for the tubes. For the functionalized, clumped tubes, at least five peaks are clearly resolvable at 192.6, 214.8, 231.8, 254.1, and 280.5 cm^{-1},

(41) Dresselhaus, M. S.; Dresselhuas, G.; Jorio, A.; Souza Filho, A. G.; Pimenta, M. A.; Saito, R. *Acc. Chem. Res.* **2002**, *35*, 1070.
(42) Yu, Z.; Brus, L. E. *J. Phys. Chem. B* **2001**, *105*, 1123.
(43) Kukovecz, A.; Kramberger, C.; Georgakilas, V.; Prato, M.; Kuzmany, H. *Eur. Phys. J. B* **2002**, *28*, 223.
(44) Kataura, H.; Kumazawa, Y.; Maniwa, Y.; Umezu, I.; Suzuki, S.; Ohtsuka, Y.; Achiba, Y. *Synth. Met.* **1999**, *103*, 2555.
(45) Kavan, L.; Rapta, P.; Dunsch, L.; Bronikowski, M. J.; Willis, P.; Smalley, R. E. *J. Phys. Chem. B* **2001**, *105*, 10764.

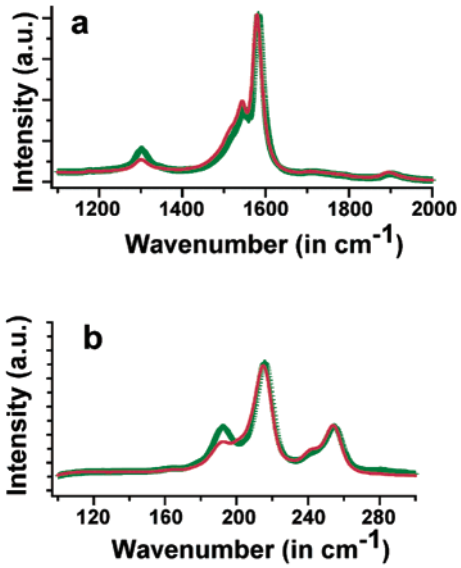

Figure 7. Raman spectra collected at 632.8 nm excitation of purified tubes (green markers) and OsO_2-derivatized tubes (red). (a) G and D band region. (b) Radial breathing mode region of spectrum with the intensity normalized at 255 cm^{-1}.

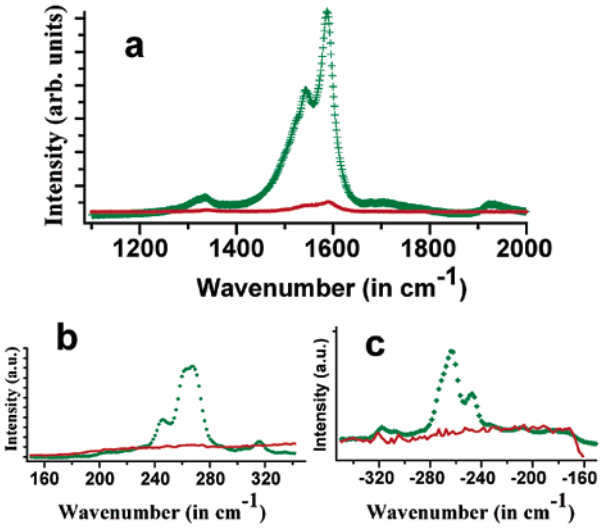

Figure 8. Raman spectra collected at 514.5 nm excitation of purified tubes (green markers) and OsO_2-derivatized tubes (red). (a) G and D band region. (b) Stokes spectra of radial breathing mode region of spectrum with the intensity normalized for the background. (c) Anti-Stokes spectra of radial breathing mode region.

respectively. These values correspond to larger tubes with diameters of 1.3, 1.16, 1.07, 0.97, and 0.88 nm, respectively.

A few conclusions can be drawn from the Raman studies shown in Figures 6 and 7. First, there is no dramatic change of the Raman spectra at laser wavelengths of 632.8 and 1064 nm upon functionalization. This indicates that the structural and electronic integrity of the primarily semiconducting nanotubes being probed is essentially conserved. Second, the most interesting features of our Raman data relate to subtle changes in the RBM profiles, particularly evident at 632.8 nm irradiation.

A decrease[46] in the intensity of the RBM bands has been known to be suggestive of moiety bonding along the sidewalls. In Figure 7b, upon intensity normalization at 255 cm^{-1}, it is apparent that for the functionalized adducts there is a selective reduction in the intensity of the lowest frequency Raman band, corresponding to the larger diameter (~1.3 nm) tubes. That is, the lowest frequency RBM band, which can also be attributed to (13, 4) and (9, 9) metallic tubes, is attenuated with respect to the other bands in the RBM region. Since there was no net loss of tubes from the reaction mixture before and after chemical derivatization, the data suggest that the larger diameter tubes, as opposed to ostensibly more reactive smaller diameter tubes, are more affected by the functionalization process. How can this be explained?

One plausible mechanism recently proposed is that these largest tubes, whose intensities are attenuated, are metallic ones, as deduced from a revised Kataura plot.[21,22,44] This would be indicative of the selective functionalization of metallic nanotubes over smaller diameter semiconducting nanotubes. Nonetheless, the net result is a loss of resonance enhancement of the Raman spectra for the metallic nanotubes, thereby accounting for the observed attenuation in peak intensity.[47]

In this experiment, because of the preponderance of OsO_2 species observed in the product by XPS analysis, the reaction process likely involves (a) intercalation involving transport of the reactants to the nanotube sidewalls followed by (b) subsequent reduction of OsO_4 to OsO_2 with a net transfer of electrons from the nanotubes to the Os(VIIII) species. It is believed that this net process involves the formation of an intermediate charge-transfer complex with the metallic nanotubes, a hypothesis we explore further on. In general, extraction and transfer of electrons by the formation of a covalent bond has been shown to occur more facilely for metallic tubes rather than for semiconducting tubes.[21,22] The origin of this selectivity is expected to arise from the ease of formation of a charge-transfer complex. To summarize the Raman data, there is an intensity loss in the RBM modes corresponding to the thickest tubes, permitting us to rule out RBM band shifting as a likely cause and suggesting that functionalization occurs predominantly with the largest metallic tubes, leaving the semiconducting tubes unaffected.

To further confirm this assertion, namely the high chiral and size selectivity of this chemical reaction, we obtained Raman data (Figure 8) at 514.5 nm (2.41 eV) excitation where predominantly smaller-diameter metallic tubes are in resonance.[20,24] Prominent bands are centered at 245.9, 262.4, 268.0, and 316.3 cm^{-1}, which are described in more extensive detail in previous Raman studies[20,48] at this wavelength. It is evident that the metallic tubes observed in resonance here have higher RBM values than what we have observed at 632.8 nm and, hence, are smaller in diameter. On functionalization, the change in intensity is undeniable. The peaks corresponding to derivatized, osmylated nanotubes are greatly reduced in intensity, and most of the RBMs in the Stokes and anti-Stokes have dramatically decayed. On normalization, there is also seen to be an increase in the intensity of the D band relative to the G band of the functionalized tubes. Such a sharp, complete decrease in the resonances for the metallic tubes at 514.5 nm, as compared with the comparatively minimal alterations observed with the

(46) Marcoux, P. R.; Schreiber, J.; Batail, P.; Lefrant, S.; Renouard, J.; Jacob, G.; Albertini, D.; Mevellec, J.-Y. *Phys. Chem. Chem. Phys.* **2002**, *4*, 2278.
(47) Bendiab, N.; Anglaret, E.; Bantignies, J.-L.; Zahab, A.; Sauvajol, J.-L.; Petit, P.; Mathis, C.; Lefrant, S. *Phys. Rev. B* **2001**, *64*, 245424.
(48) Strano, M. S.; Doorn, S. K.; Haroz, E. H.; Kittrell, C.; Hauge, R. H.; Smalley, R. E. *Nano Lett.* **2003**, *3*, 1091.

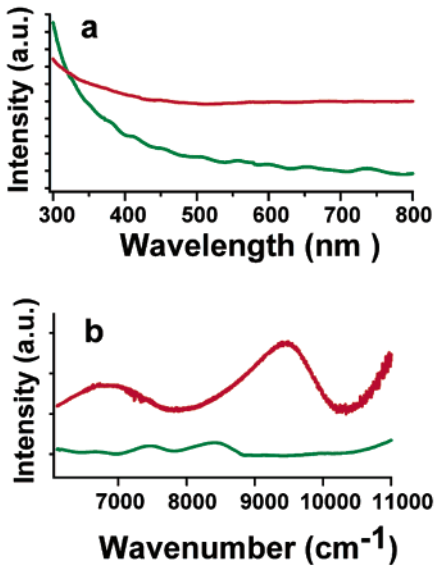

Figure 9. (a) UV−visible spectra of unprocessed HiPco SWNTs (green) and of OsO_2-functionalized nanotubes (red). The vertical axis is intensity in arbitrary units. (b) Near-IR spectra of purified HiPco (green) and of OsO_2-functionalized nanotubes (red).

peaks of primarily semiconducting tubes at 632.8 nm, provides excellent evidence for the selective functionalization[21,22] of metallic tubes by osmium tetroxide, consistent with the data presented previously.

Further Optical Observations. As has been mentioned, the electronic density of states of SWNTs possesses spike-like features known as van Hove singularities. Optically allowed transitions between these features can be observed in the UV−near-IR spectral region[1] for raw HiPco nanotubes (Figure 9). The primary features are transitions between the first pair of singularities (M_{11}) in metallic tubes as well as S_{11} and S_{22}, the transitions between the first and second pairs of singularities for the semiconducting tubes.

Figure 9a shows that the osmium dioxide coated adducts do not show the M_{11} transitions and that the optical spectra of the functionalized adduct are mostly featureless in the region of interest. The loss of the UV transitions in the M_{11} region is consistent with the presence of covalent sidewall functionalization disrupting the electronic structure of metallic nanotubes. That is, covalent functionalization, through the mediation of cycloaddition of osmium tetroxide, essentially saturates the bond structure on the nanotube sidewalls, introducing defects that perturb and destroy the periodicity of the intrinsic conjugated sp^2-hybridized electronic structure of the nanotube.[10,14,49] Indeed, this loss of conjugation could be the primary reason for the decrease in conductivity that has been observed upon the interaction of metallic carbon nanotubes with OsO_4 vapor.[31b]

FT-near-IR measurements (Figure 9b) of the functionalized, osmylated nanotubes show peaks near the 0.9 eV region, corresponding to transitions between the first set of singularities in the semiconducting tubes. The transitions of the functionalized tubes are shifted from those of the purified tubes, likely due to a change in tube bundling characteristics upon reaction and to the presence of a thick OsO_2 coating on the tubes. Thus far, we have not fully ruled out the interaction of nanotubes with OsO_4 as a potential noncovalent doping process[50] of nanotubes in analogy to p-doping of nanotubes by $FeCl_3$ intercalation, which tends to preferentially affect the larger tubes due to their wider intertube channels[51−53] and which would have shifted the Fermi level of the nanotube,[51] thereby rendering certain transitions as optically forbidden.[54,55] Indeed, noncovalent doping interactions can account for the observed bleaching of optical transitions and loss of Raman resonance features. However, doping interactions tend to bleach band-gap transitions in order of increasing energy.[45,49,56]

It is evident from Figure 9 that for the functionalized, osmylated tubes, we have retained the lower energy S_{11} transitions at ∼0.9 eV but lost the higher energy M_{11} transitions, so a doping mechanism certainly cannot be an adequate explanation. Rather, these observations coupled together with the observed greater loss of Raman resonance for metallic nanotubes, as compared with the mainly unaffected semiconducting transitions, further support the case that the loss of UV−visible−near-infrared optical transitions likely arises from selective covalent sidewall functionalization of primarily metallic nanotubes.[21,22] It is of note that reactions at ends and defect sites alone cannot account for the dramatic decay of Raman resonances and loss of band-gap transitions noted here, providing further evidence that the reaction likely occurs on the metallic nanotube sidewalls.

Mechanistic Insights into Nanotube Osmylation: Formation of Charge-Transfer Complex. An important point to mention is that UV irradiation is absolutely critical to the formation of the structures presented in Figures 1−4. When the experimental protocol, for instance, was carried out in the absence of UV irradiation, none of the thickly coated ropes, characteristic of a typical reaction, were observed. In addition, these processed nanotubes retained the optical transitions between the van Hove singularities.

Furthermore, another control experiment was carried out in the presence of base (i.e., pyridine) but without UV irradiation. After a few days of stirring, the resulting tubes appeared remarkably clean. Though a very low density of osmium clusters, from EDS measurements, was observable on the nanotube surface, the expected optical features of the nanotubes were retained, implying a lack of alteration in the intrinsic electronic structure of the tubes. Also, none of the unique morphological structures, apparent in Figures 1−4, were observed. XPS analysis identified the oxidation states of the osmium in the complexes observed in this control experiment as consisting of a mixture of +8, +6, and +4.

To better understand the nature of the osmylation reaction with nanotubes and the necessity of UV irradiation, we discuss a potential reaction mechanism in relation to analogous charge-transfer (CT) osmylation reactions of benzenoid hydrocarbons.[57,58] It should be mentioned, though, that the reaction

(49) Kamaras, K.; Itkis, M. E.; Hu, H.; Zhao, B.; Haddon, R. C. *Science* **2003**, *301*, 1501.
(50) Duclaux, L. *Carbon* **2002**, *40*, 1751.
(51) Pichler, T.; Kukovecz, A.; Kuzmany, H.; Kataura, H. *Synth. Met.* **2003**, *135−136*, 717.
(52) Kukovecz, A.; Pichler, T.; Pfeiffer, R.; Kramberger, C.; Kuzmany, H. *Phys. Chem. Chem. Phys.* **2003**, *5*, 582.
(53) Kukovecz, A.; Pichler, T.; Pfeiffer, R.; Kuzmany, H. *Chem. Commun.* **2002**, 1730.
(54) Rao, A. M.; Eklund, P. C.; Bandow, S.; Thess, A.; Smalley, R. E. *Nature* **1997**, *388*, 257.
(55) Rao, A. M.; Bandow, S.; Richter, E.; Eklund, P. C. *Thin Solid Films* **1998**, *331*, 141.
(56) Petit, P.; Mathis, C.; Journet, C.; Bernier, P. *Chem. Phys. Lett.* **1999**, *305*, 370.

Scheme 1. Osmylation of Anthracene Derivatives,[58] Analogous to Nanotube Osmylation

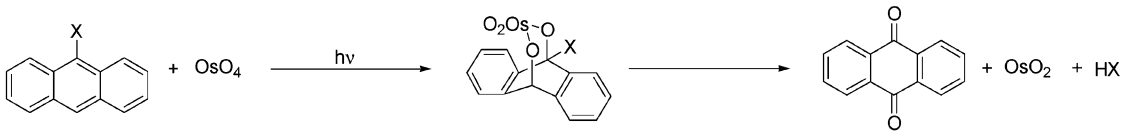

mechanisms for these reactions are not exactly identical. For instance, whereas solutions of complexes of OsO_4 and most aromatic donors possess characteristic CT absorption bands,[57,58] it is difficult to observe a distinctive charge-transfer band in our heterogeneous nanotube reaction mixture.

In the current reaction, the mixture is photochemically excited at 254 nm, corresponding to the $A_1 \rightarrow T_2$ ($3t_2 \rightarrow 2e$) transition, the second dipole-allowed transition in OsO_4.[59] When OsO_4 is activated from the ground to the excited T_2 state, it becomes a much better oxidizing agent and can more readily accept electrons. Osmium tetroxide is a versatile electron acceptor with alkenes and arenes, and by analogy, it is highly probable that the first step of our reaction process involves the formation of an electron donor−acceptor (EDA) complex[58] with the nanotube. These types of complexes with most arenes are weak and can easily dissociate. A reasonable structure for the analogous short-lived ion pair state involving the nanotube is shown in eq 3.

$$\mathrm{NT} + \mathrm{OsO_4} \rightarrow [\mathrm{NTOsO_4}] \rightarrow \mathrm{NT^+OsO_4^-} \qquad (3)$$

How easily would this transient intermediate form? The formation of this intimate ion pair necessitates a loss of electrons from the nanotube, thereby depleting the valence band states. An important measure of the ability of any molecule or molecular entity to give up electrons is its ionization potential. With benzenoid hydrocarbons, the formation of arene cations occurs with arenes, possessing ionization potentials of up to 9.23 eV (benzene). A particularly stable cation is formed with the electron-rich 9,10-dimethylanthracene,[60] with an ionization potential of 7.11 eV. By comparison with these arenes, the ionization potential of (5, 5) SWNTs is estimated to be much more favorable at 6.4 eV and can be further reduced upon water adsorption.[61] Ionization potentials for (4, 4) SWNTs were found to be about 6.0 eV.[62] Thus, as compared with arenes, it should be relatively facile for nanotubes to give up electrons to an excited OsO_4.

The facility of formation of the charge-transfer complex involving the nanotube and the extent of electron transfer from the nanotube surface to the osmium tetroxide species are expected to be highly dependent on the electron density near the Fermi level.[21,22] Thus, metallic and semimetallic nanotubes, as compared with semiconducting tubes, are expected to have a higher reactivity toward and a greater ability to reduce an excited OsO_4. Hence, the electronic density of states of the nanotubes is capable of influencing the relative reactivity of metallic and semiconducting nanotubes by preferentially stabilizing the transition state shown in eq 3.

Control experiments, run in the absence of nanotubes from the reaction mixture, indicated a lack of deposition of OsO_2 precipitate even after more than 2 h of UV irradiation. Moreover, the structures, seen in Figures 1−4, are not observed if toluene is substituted by the base, pyridine, in the reaction mixture. This observation is consistent with the proposed formation of an EDA complex (eq 3), as preferential coordination of the Lewis base pyridine with the electron acceptor ($K \sim 48\ \mathrm{M^{-1}}$) would have disrupted the EDA complex.[58] This is an important difference from a theoretical prediction of osmate ester formation,[31a] which postulates a straightforward [2 + 3] cycloaddition reaction. Rather, experimental nanotube osmylation is far more analogous to a photoactivated charge-transfer process, observed previously for benzenoid hydrocarbons.[57,58] The absolute requirement for UV irradiation in this reaction underscores the importance of the initial formation of the EDA charge-transfer complex.

Ion pairs with arenes will spontaneously collapse and undergo cycloaddition.[57,58] By analogy, for nanotubes, the intermediate transition state, strongly stabilized in the case of metallic tubes by electron donation, will be similarly subjected to covalent cycloaddition from osmium tetroxide. The introduction of covalent bonds on a nanotube surface increases the reactivity of adjacent carbons. An analogous reaction mechanism involving the loss of electrons from metallic tubes through the formation of a covalent bond has been proposed for the functionalization of nanotubes with diazonium salts.[21]

To illustrate the viability of the mechanistic possibility of charge transfer with nanotubes, charge-transfer osmylation of anthracene in nonpolar solvents can lead to the oxidation of anthracene to anthraquinone and the subsequent generation of OsO_2, as shown in Scheme 1.[58]

We believe that, by analogy, a very similar type of reaction occurs with metallic nanotubes. The coordinately unsaturated OsO_2, precipitated out, can then self-aggregate to form the thick coating observed on the tubes (Figures 1−4).

To summarize, we postulate electron transfer from the nanotube to OsO_4 in a process promoted by UV irradiation. In the absence of UV irradiation, the intermediate charge-transfer state is probably more difficult to form. As it is, an intermediate charged ion pair state forms and dissociates at the nanotube sidewalls, though we cannot rule out possible reaction at defect sites as well. In the process, the nanotube provides electrons for the reduction of OsO_4 to OsO_2. Electron donation from the nanotube stabilizes the creation of an intermediate complex and formation of a covalent bond at the nanotube sidewalls. The coordinately unsaturated OsO_2 can then continue to polymerize on the surfaces of the bundles and in the cavities of the intertube channels. The intertube channels, particularly of larger tubes, are reasonable sites for the growth of the small crystalline cores seen in the HRTEM images.

We ascribe coverage and clumping onto sidewall surfaces of the tubes with large quantities of OsO_2 as the causative explanation for the large metal-functionalized aggregates observed in Figures 1, 2, and 4. Since the reaction proceeds by

(57) Wallis, J. M.; Kochi, J. K. *J. Org. Chem.* **1988**, *53*, 1679.
(58) Wallis, J. M.; Kochi, J. K. *J. Am. Chem. Soc.* **1988**, *110*, 8207.
(59) Roebber, J. L.; Wiener, R. N.; Russell, C. A. *J. Chem. Phys.* **1974**, *60*, 3166.
(60) Masnovi, J. M.; Seddon, E. A.; Kochi, J. K. *Can. J. Chem.* **1984**, *62*, 2252.
(61) Maiti, A.; Andzelm, J.; Tanpipat, N.; von Allmen, P. *Phys. Rev. Lett.* **2001**, *87*, 155502.
(62) Hou, S.; Shen, Z.; Zhao, X.; Xue, Z. *Chem. Phys. Lett.* **2003**, *373*, 308.

the intermediate formation of an electron-rich charge-transfer complex, the osmylation reaction observed here with SWNTs is chirality selective, favoring reactivity involving metallic tubes over semiconducting tubes. The formation of a thick OsO_2 coating on the metallic nanotube surfaces likely saturates the nanotube sidewalls, rendering them inaccessible to further reaction with incoming OsO_4 reagent, thereby preventing covalent sidewall functionalization of the less reactive semiconducting nanotubes.

Conclusions

The interaction of solution-phase OsO_4 with SWNTs in the presence of UV irradiation demonstrates chemical specificity toward nanotube electronic structure. Nanotube osmylation appears to be chemically selective in differentiating between the reactivity of metallic vs semiconducting nanotubes. That is, metallic nanotubes, with a larger electron density near the Fermi level, are better able to stabilize an intermediate charge-transfer complex with an excited OsO_4 species. When the charge-transfer complex dissociates, the net results are (a) covalent sidewall functionalization of these nanotubes through disruption of the conjugated π-electron structure as well as (b) reduction of the osmium tetroxide species to OsO_2 nanoparticles, which are then templated onto the sidewall surface. A systematic Raman study of our nanotube samples at three different excitation wavelengths, probing different electronic populations of tubes, provides strong evidence of the higher reactivity of metallic tubes with respect to osmylation. These observations bear out a theoretical prediction of covalent sidewall osmylation of nanotubes. In addition, in contrast to noncovalent wrapping reactions, electrochemical processes, and electron-beam evaporation techniques used to achieve similar results,[63−65] this work represents the first example of nanoparticulate templating onto SWNT surfaces, through the mediation of covalent chemistry. In fact, the templating of OsO_2 on metallic nanotube surfaces may serve as the basis for achieving chiral separation of these nanotubes through centrifugation based on density differences.

Nanotube osmylation, based on differential reactivity of nanotube species, holds promise for the selection of nanotubes of particular electronic structure and size, essential for applications such as the development of nanotube-based electrodes as well as advances in molecular electronics. Indeed, the reactivity observed in this work should not only provide the basis for chirality- and site-selective nanochemistry and self-assembly applications (such as the fabrication of nanotube-based composites) but also enable a means of altering the known electronic, optical, and mechanical properties of SWNTs in a controllable manner.

Acknowledgment. We acknowledge support of this work through startup funds provided by the State University of New York at Stony Brook as well as Brookhaven National Laboratory. Acknowledgment is also made to the donors of the Petroleum Research Fund, administered by the American Chemical Society, for support of this research. S.S.W. thanks 3M for a nontenured faculty award. We also thank Professor Jianyu Huang (Department of Physics, Boston College) and Dr. James Quinn (Materials Science, SUNY at Stony Brook) for their help with HRTEM and SEM/TEM analyses, respectively. The assistance of Dr. Alasdair Bell and Professor Peter Tonge with Raman analyses at 632.8 nm and with the use of their UV lamp is much appreciated. Dr. Arthur Sedlacek is thanked for his help with solution-phase FT-Raman work. We are grateful to Professor Albert Haim for helpful discussions. Drew Hirt (Materials Research Laboratories, Inc.) and Franklin D. Hardcastle (NAMAR Scientific, Inc.) are acknowledged for their work with the XPS results and with the Raman analyses at 514.5 nm. We are particularly indebted to an anonymous reviewer for very thoughtful comments on the interpretation of our Raman data.

JA038111W

(63) Fischer, J. E. *Acc. Chem. Res.* **2002**, *35*, 1079.
(64) Zhang, Y.; Dai, H. *Appl. Phys. Lett.* **2000**, *77*, 3015.
(65) Zhang, Y.; Franklin, N. W.; Chen, R. J.; Dai, H. *Chem. Phys. Lett.* **2000**, *331*, 35.